Available online at www.sciencedirect.com
ScienceDirect
Journal of Organometallic Chemistry 692 (2007) 2205–2215
Journal of Organometallic Chemistry
www.elsevier.com/locate/jorganchem

Synthesis, crystal structures and third-order nonlinear optical properties of a new family of double incomplete cubane-like clusters $[(\eta^5\text{-}C_5Me_5)_2Mo_2(\mu_3\text{-}S)_3SCu_2X(\mu\text{-}X)]_2$ ($X = Cl^-$, Br^-, SCN^-) and cubane-like clusters $[(\eta^5\text{-}C_5Me_5)_2Mo_2(\mu_3\text{-}S)_4(CuX)_2]$ ($X = Br^-$, SCN^-, CN^-)

Zhi-Gang Ren [a,b], Hong-Xi Li [a], Ling-Ling Li [a], Yong Zhang [a], Jian-Ping Lang [a,b,*], Jun-Yi Yang [c], Ying-Lin Song [c,*]

[a] School of Chemistry and Chemical Engineering, Suzhou University, Suzhou 215123, Jiangsu, People's Republic of China
[b] State Key Laboratory of Organometallic Chemistry, Shanghai Institute of Organic Chemistry, Chinese Academy of Sciences, Shanghai 200032, People's Republic of China
[c] School of Physical Science and Technology, Suzhou University, Suzhou 215006, Jiangsu, People's Republic of China

Received 11 December 2006; received in revised form 19 January 2007; accepted 23 January 2007
Available online 30 January 2007

Abstract

Reactions of *trans*-$[(\eta^5\text{-}C_5Me_5)_2Mo_2(\mu\text{-}S)_2S_2]$ (**1**) with 2 equiv. of CuX ($X = Cl^-$, Br^-, SCN^-, CN^-) in refluxing acetonitrile resulted in a new set of Mo/Cu/S cluster compounds $[(\eta^5\text{-}C_5Me_5)_2Mo_2(\mu_3\text{-}S)_3SCu_2Cl(\mu\text{-}Cl)]_2$ (**2**), $[(\eta^5\text{-}C_5Me_5)_2Mo_2(\mu_3\text{-}S)_4(CuBr)_2]$ (**3**) and $[(\eta^5\text{-}C_5Me_5)_2Mo_2(\mu_3\text{-}S)_3SCu_2Br(\mu\text{-}Br)]_2$ (**4**), $[(\eta^5\text{-}C_5Me_5)_2Mo_2(\mu_3\text{-}S)_4(CuSCN)_2]$ (**5**) and $[(\eta^5\text{-}C_5Me_5)_2Mo_2(\mu_3\text{-}S)_3SCu_2(SCN)(\mu\text{-}SCN)]_2$ (**6**) and $[(\eta^5\text{-}C_5Me_5)_2Mo_2(\mu_3\text{-}S)_4(CuCN)_2]$ (**7**). Compounds **2**–**7** were fully characterized by elemental analysis, IR, UV–Vis, ^1H NMR and single-crystal X-ray crystallography. Compounds **2**, **4** and **6** consist of two incomplete cubane-like $[(\eta^5\text{-}C_5Me_5)_2Mo_2(\mu_3\text{-}S)_3SCu_2X]$ species bridged by a pair of $\mu\text{-}X^-$ anions while **3**, **5** and **7** contain a cubane-like $[(\eta^5\text{-}C_5Me_5)_2Mo_2(\mu_3\text{-}S)_4Cu_2]$ core with each of two terminal X^- coordinated at each copper(I) center. The third-order nonlinear optical (NLO) properties of **2**–**5** and **7** along with $[(\eta^5\text{-}C_5Me_5)_2Mo_2(\mu_3\text{-}S)_4(CuCl)_2]$ in CH_2Cl_2 were investigated by using *Z*-scan technique at 532 nm. All these clusters showed strong third-order NLO absorption effects and self-defocusing properties.

Keywords: Molybdenum; Copper; Cluster; Sulfide; Molecular structures; Third-order nonlinear optical properties

1. Introduction

The reactions of thiomolybdates and thiotungstates $[MO_{4-n}S_n]^{2-}$ and $[(\eta^5\text{-}C_5Me_5)MS_3]^-$ (M = Mo, W) with copper(I) salts have been extensively investigated due to their rich chemistry [1–27], and their relations to biological systems [1,5,6,28,29], and electro/photonic materials [11,15,16,24,26,30–39]. However, only a few reactions are involved in the utilization of the disulfido-bridged dimolybdenum clusters $[Cp'_2Mo_2S_4]$ ($Cp' = \eta^5\text{-}C_5H_5$, $\eta^5\text{-}C_5H_4Me$ or $\eta^5\text{-}C_5Me_5$) [40,41]. For example, reactions of a solution containing *trans*-$[(\eta^5\text{-}C_5Me_5)_2Mo_2(\mu\text{-}S)_2S_2]$ (**1**) with 2 equiv. of CuCl in toluene gave rise to a cubane-like cluster $[(\eta^5\text{-}C_5Me_5)_2Mo_2(\mu_3\text{-}S)_4(CuCl)_2]$ [40].

On the other hand, we have been interested in the synthesis of Mo(W)/Cu/S clusters derived from $[MO_{4-n}S_n]^{2-}$ and $[(\eta^5\text{-}C_5Me_5)MS_3]^-$ (M = Mo, W) [13,14,16–27,30–32,39]. Some of these clusters exhibited good third-order nonlinear

* Corresponding authors. Tel.: + 86 512 6588 2865; fax: + 86 512 6588 0089 (J.-P. Lang).
E-mail address: jplang@suda.edu.cn (J.-P. Lang).

0022-328X/$ - see front matter © 2007 Elsevier B.V. All rights reserved.
doi:10.1016/j.jorganchem.2007.01.040

optical (NLO) properties in solution [16,26,30–32,36,37,39]. In order to expand the chemistry of Mo(W)/Cu/S clusters and screen out clusters with better NLO performances, we have became to adopt other Mo(W)/S precursors including **1** [41–43]. In fact, we have recently reported that treatment of a suspension of **1** in methylene dichloride with 2 equiv. of CuI at ambient temperature afforded an incomplete cubane-like cluster $[(\eta^5\text{-}C_5Me_5)_2Mo_2(\mu_3\text{-}S)_3S(CuI)_2]$ while a *cis*-isomer $[(\eta^5\text{-}C_5Me_5)_2Mo_2(\mu_3\text{-}S)_4(CuI)_2]$ could be isolated through heating $[(\eta^5\text{-}C_5Me_5)_2Mo_2(\mu_3\text{-}S)_3S(CuI)_2]$ either in solution or in solid state [41]. Interestingly, both clusters in CH_2Cl_2 showed better NLO effects than those of their cluster precursor **1**. The results encouraged us to further explore reactions of **1** with other copper(I) halides or pseudohalides CuX (X = Cl, Br, SCN, CN) systemically and the third-order NLO properties of the resulting products. In this paper, we report syntheses, crystal structures and third-order NLO properties of a new family of double incomplete cubane-like clusters and cubane-like clusters derived from **1**: $[(\eta^5\text{-}C_5Me_5)_2Mo_2(\mu_3\text{-}S)_3SCu_2Cl(\mu\text{-}Cl)]_2$ (**2**), $[(\eta^5\text{-}C_5Me_5)_2Mo_2(\mu_3\text{-}S)_4(CuBr)_2]$ (**3**) and $[(\eta^5\text{-}C_5Me_5)_2Mo_2(\mu_3\text{-}S)_3SCu_2Br(\mu\text{-}Br)]_2$ (**4**), $[(\eta^5\text{-}C_5Me_5)_2Mo_2(\mu_3\text{-}S)_4(CuSCN)_2]$ (**5**) and $[(\eta^5\text{-}C_5Me_5)_2Mo_2(\mu_3\text{-}S)_3SCu_2(SCN)(\mu\text{-}SCN)]_2$ (**6**) and $[(\eta^5\text{-}C_5Me_5)_2Mo_2(\mu_3\text{-}S)_4(CuCN)_2]$ (**7**).

2. Results and discussion

2.1. Synthesis and spectral characterization of 2–7

Treatment of **1** with 2 equiv. of CuCl in refluxing CH_3CN followed by a standard workup afforded the known single cubane-like cluster $[(\eta^5\text{-}C_5Me_5)_2Mo_2(\mu_3\text{-}S)_4(CuCl)_2]$ (33% yield) and a new double incomplete cubane-like cluster **2** (51% yield) (Scheme 1). Similar reactions of **1** with 2 equiv. of CuBr produced **3** and **4** in 46% and 30% yields, respectively. It is noticed that the double incomplete cubane-like cluster **2** or **4** gradually underwent the *trans*-to-*cis* isomerization [41] to form the cubane-like cluster $[(\eta^5\text{-}C_5Me_5)_2Mo_2(\mu_3\text{-}S)_4(CuX)_2]$ (X = Cl, Br (**3**)) during the reaction period. For example, reactions of **4** in refluxing CH_3CN for 20 h followed by column chromatography on silica gave rise to a mixture of **3** (38% yield) and **4** (57% yield). Continuous heating of this solution of **4** did not significantly increase the yield of **3** (41% yield) but **4** (48% yield) became decomposed after a heating period of 40 h and some unknown species occurred in the ^1H NMR spectra. Similar phenomena were once observed in their iodide analogue [41], though **2** or **4** may be cleaved into 2 equiv. of incomplete cubane-like $[(\eta^5\text{-}C_5Me_5)_2Mo_2(\mu_3\text{-}S)_3S(CuX)_2]$ clusters before the isomerization.

Intriguingly, analogous reactions of **1** with 2 equiv. of CuSCN gave rise to the single cubane-like cluster **5** in 31% yield coupled with the double incomplete cubane-like cluster **6** (~2% yield) (Scheme 1). In the case of CuCN, no expected double incomplete cubane-like cluster $[(\eta^5\text{-}C_5Me_5)_2Mo_2(\mu_3\text{-}S)_3SCu_2(CN)(\mu\text{-}CN)]_2$ but only the cubane-like cluster **7** was isolated in 23% yield. In both cases, the yield for the double incomplete cubane-cluster was quite low, which may be attributed to the formation of a large amount of insoluble dark brown solids during the reaction. Short reaction time (2–3 h) or running the reactions at low temperatures (e.g. 0 °C) did not improve the yield for the double incomplete cubane-like cluster **6**. It is understandable that both SCN^- and CN^- are versatile bridging ligands that may link some Mo/Cu/S cluster species existed in the reaction mixture to form certain kinds of insoluble Mo/Cu/S cluster-based coordination polymers [18,27,44]. In fact, the IR spectra revealed that these solids contained the SCN^- (2118/2073 cm^{-1}) or CN^- (2129/2117 cm^{-1}) stretching vibrations and the bridging Mo–S vibration at 427 or 453 cm^{-1}. X-ray fluorescence analysis conformed that these samples contained Mo, Cu and S elements (Mo:Cu:S = 2:2:6 for X = SCN^- and 2:2:4 for X = CN^-). However, numerous attempts to grow their single crystals to elucidate their actual compositions failed.

Compounds **2**–**7** are readily soluble in CH_2Cl_2 or $CHCl_3$, slightly soluble in CH_3CN, benzene or acetone,

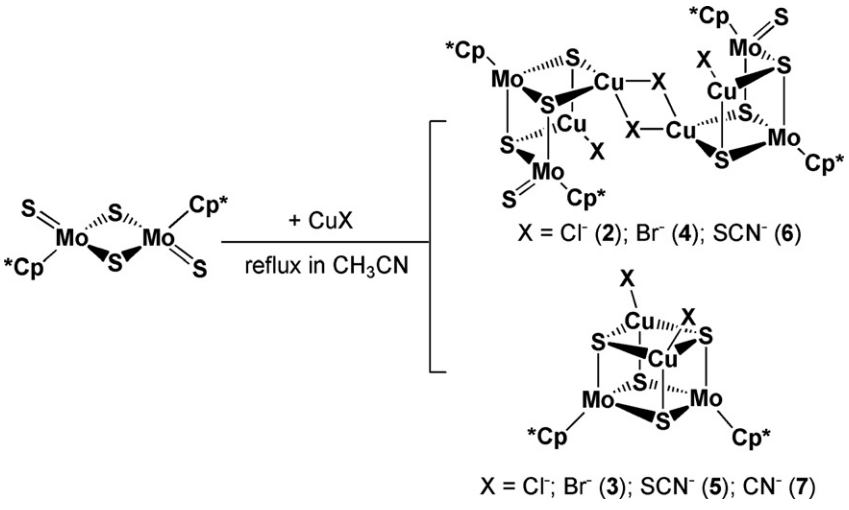

Scheme 1.

and insoluble in Et_2O and hexane. The CH_2Cl_2 solvated molecules in $\mathbf{3}\cdot 0.5CH_2Cl_2$ and $\mathbf{7}\cdot CH_2Cl_2$ could be readily removed in vacuo at ~60 °C. The elemental analyses were consistent with the chemical formulas of **2**, $\mathbf{3}\cdot 0.5CH_2Cl_2$, **4**–**6** and $\mathbf{7}\cdot CH_2Cl_2$. In the IR spectra of **2**, **4** and **6**, bands at 503 (**2**), 503 (**4**), and 498 (**6**) cm^{-1} and 428 (**2**), 428 (**4**), and 455 (**6**) cm^{-1} may be assigned as the terminal Mo = S and the bridging Mo–S stretching vibrations, respectively [41,45]. The IR spectra of **3**, **5** and **7** showed only one bridging Mo–S stretching vibration at 451 (**3**), 454 (**5**), and 455 (**7**) cm^{-1}. Compounds **5**, **6** and **7** also exhibited the stretching vibrations of SCN^- or CN^- at 2093 (**5**), 2115/2078 (**6**), and 2154/2087 (**7**) cm^{-1}, respectively. The UV–Vis spectra of **2** and **4** in CH_2Cl_2 were characterized by four bands, while those of **3**, **5** and **6** had three absorptions and that of **7** had two absorptions (Fig. 1). Relative to the bands at 338 and 448 nm (**1**) [40], those at 350 and 491 nm (**2**), 393 and 474 nm (**3**), 352 and 491 nm (**4**), 387 and 468 nm (**5**), 469 nm (**6**), and 456 nm (**7**) are red-shifted, and they are probably dominated by the S → Mo(V) charge-transfer transitions of $[(\eta^5\text{-}C_5Me_5)_2Mo_2S_4]$ moiety [41,46]. The ^1H NMR spectra of **2**, **4**, and **6** showed two sharp singlets related to protons of two $\eta^5\text{-}C_5Me_5$ groups at 2.06 and 2.29 ppm (**2**), 2.06 and 2.28 ppm (**4**) and 2.06 and 2.17 ppm (**6**), while those of **3**, **5** and **7** presented only one single resonance of $\eta^5\text{-}C_5Me_5$ groups at 2.09 ppm (**3**), 2.12 (**5**), and 2.08 ppm (**7**). The identities of **2**, $\mathbf{3}\cdot 0.5CH_2Cl_2$, **4**–**6** and $\mathbf{7}\cdot CH_2Cl_2$ were further confirmed by single crystal X-ray analysis.

2.2. Crystal structures of $[(\eta^5\text{-}C_5Me_5)_2Mo_2(\mu_3\text{-}S)_3SCu_2X(\mu\text{-}X)]_2$ (*2*: X = Cl, *4*: X = Br; *6*: X = SCN)

Being crystallized in the monoclinic space group $P2_1/c$, the asymmetric unit for either **2** or **4** or **6** consists of half of the discrete molecule $[(\eta^5\text{-}C_5Me_5)_2Mo_2(\mu_3\text{-}S)_3SCu_2X(\mu\text{-}X)]_2$ (X = Cl (**2**); X = Br (**4**); X = SCN (**6**)). Their cell parameters of **2** and **4** are essentially identical, and so are their molecular structures. Therefore only the perspective views of **4** and **6** are shown in Figs. 2 and 3. Selected bond lengths and angles for **2**, **4** and **6** are compared in Table 1. X-ray diffraction analysis confirmed that **2** or **4** or **6** has a dimeric structure that is composed of two incomplete cubane-like $[(\eta^5\text{-}C_5Me_5)_2Mo_2(\mu_3\text{-}S)_3SCu_2X]$ fragments linked by two μ-X atoms. A crystallographic inversion center is located at the center of the cluster. These dimeric structures resemble those found in $(PPh_4)_2[(\eta^5\text{-}C_5Me_5)_2M(\mu_3\text{-}S)_3Cu_3X_2(\mu\text{-}X)]_2$ (M = Mo, X = Br; M = W, X = Cl, Br), which contains two incomplete cubane-like $[(\eta^5\text{-}C_5Me_5)_2M(\mu_3\text{-}S)_3Cu_3X_2]$ fragments interconnected by a pair of bridging X^- groups. In the case of thiocyanate clusters, the structure of **6** is different from that of $(PPh_4)_2[(\eta^5\text{-}C_5Me_5)_2M(\mu_3\text{-}S)_3Cu_3X_2(\mu\text{-}X)]_2$, in which each of the two triply-bridging SCN^- groups link three Cu(I) centers of the other $[(\eta^5\text{-}C_5Me_5)_2M(\mu_3\text{-}S)_3Cu_3(SCN)_2]$ fragment to form a double cubane-like structure.

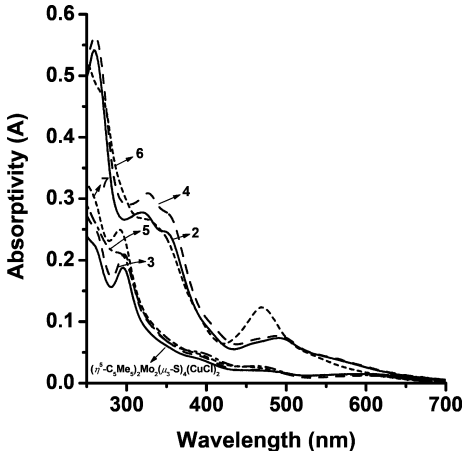

Fig. 1. Electronic spectra of $[(\eta^5\text{-}C_5Me_5)_2Mo_2(\mu_3\text{-}S)_4(CuCl)_2]$ (0.9×10^{-5}M), **2**–**6** (1.0×10^{-5} M) and **7** (1.2×10^{-5}M) in CH_2Cl_2 in a 1 cm thick glass cell.

In each $[(\eta^5\text{-}C_5Me_5)_2Mo_2(\mu_3\text{-}S)_3SCu_2X]$ fragment, the formal oxidation states for Cu and Mo atoms are assumed to be +1 and +5, respectively. Although the structure of each fragment is closely related to that of $[(\eta^5\text{-}C_5Me_5)_2Mo_2(\mu_3\text{-}S)_3SCu_2I_2]$, the two Cu atoms show different coordination geometries. The Cu(1) or Cu(1A) atoms is tetrahedrally coordinated by two μ_3-S atoms and two bridging X^- groups, while the Cu(2) or Cu(2A) atoms adopt an approximately trigonal planar geometry, coordinated by one terminal X^- group and two μ_3-S atoms. Because of the different coordination geometries of the two copper atoms, the Mo···Cu contacts are also different: Mo(2)···Cu(1)/Mo(2)···Cu(2) = 2.7202(9) Å/2.6462(7) Å (**2**); 2.7230(9) Å/2.6450(9) Å (**4**); 2.7100(8) Å/2.6327(8) Å (**6**), which correlate with the number of bonding interactions at Cu(I) centers. The Mo(2)···Cu(2) contact is comparable to those observed in $[(\eta^5\text{-}C_5Me_5)_2Mo_2(\mu_3\text{-}S)_3SCu_2I_2]$ [41], while the Mo(2)···Cu(1) one is longer than those in clusters containing tetrahedrally-coordinated Cu such as $[MoS_4Cu_4Py_6I_2]$ (2.658(3)–2.697(3) Å) [47] but somewhat shorter than $[Cu_3MoS_3Br](PPh_3)_3S\cdot 0.5Me_2CO$ (2.776(2)–2.840(3) Å) [2]. The Cu-μ_3-S bond lengths also reflect the mode of coordination of copper atoms: Cu(2)-μ_3-S av. 2.2215(13) Å (**2**), 2.2192(12) Å (**4**) and 2.2150(14) Å (**6**) for a trigonal geometry and Cu(1)-μ_3-S av. 2.2729(11) Å (**2**), 2.2771(11) Å (**4**) and 2.2697(14) Å (**6**) for a tetrahedral environment. The mean Cu-μ_3-S bond length in **2** (2.2472(13) Å) or **4** (2.2482(12) Å) or **6** (2.2424(14) Å) is comparable to those in $(PPh_4)_2[(\eta^5\text{-}C_5Me_5)_2Mo(\mu_3\text{-}S)_3Cu_3Br_3]_2$ (2.236(3) Å) [21] and $(PPh_4)_3[MoOS_3Cu_3Cl_3][CuCl_2]$ (2.243(2) Å) [48]. The mean Mo-μ_3-S bond length in **2** or **4** or **6** is slightly longer than those in $(PPh_4)_2[(\eta^5\text{-}C_5Me_5)_2Mo(\mu_3\text{-}S)_3Cu_3Br_3]_2$ (2.290(3) Å) and $(PPh_4)_3[MoOS_3Cu_3Cl_3][CuCl_2]$ (2.272(2) Å). The mean Mo(1)···Mo(2) contact and terminal Mo(1)=S(4) in **2** or **4**, or **6** are close to those of the corresponding ones of $[(\eta^5\text{-}C_5Me_5)_2Mo_2(\mu_3\text{-}S)_3S(CuI)_2]$. Within the CuX_2Cu frame, the Cu(1)–X(1A) and Cu(1A)–X(1) bond lengths are significantly longer than the Cu(1)–X(1) and Cu(1A)–X(1A) bonds. Therefore, the two incomplete cubes of **2**, **4**, and **6** are weakly associated.

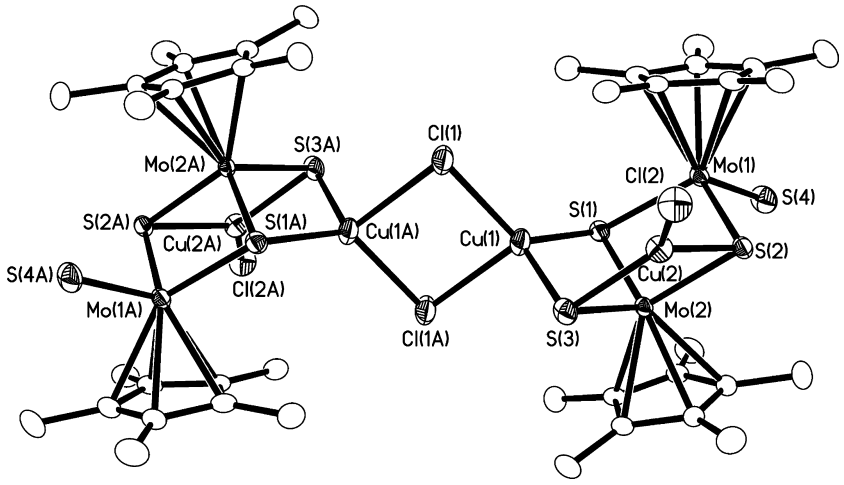

Fig. 2. Perspective view of **2** with labeling scheme and 50% thermal ellipsoids. All hydrogen atoms are omitted for charity.

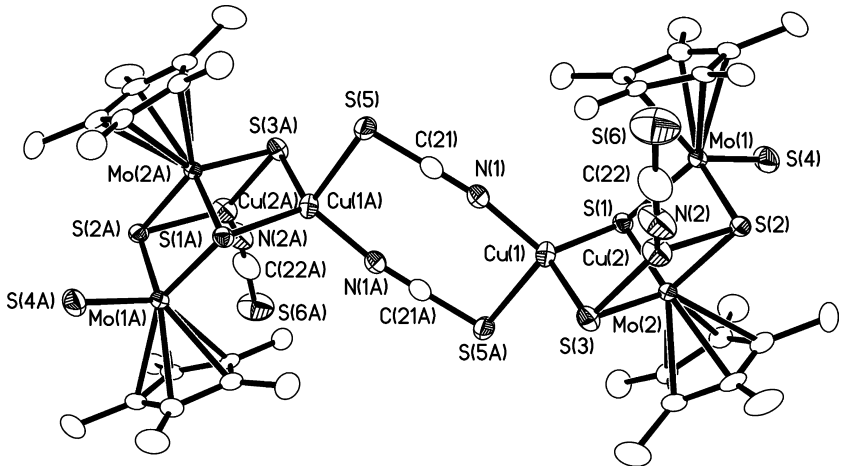

Fig. 3. Perspective view of **6** with labeling scheme and 50% thermal ellipsoids. All hydrogen atoms are omitted for charity.

*2.3. Crystal structures of $[(\eta^5\text{-}C_5Me_5)_2Mo_2(\mu_3\text{-}S)_4(CuBr)_2]\cdot 0.5CH_2Cl_2$ (**3**$\cdot 0.5CH_2Cl_2$), $[(\eta^5\text{-}C_5Me_5)_2Mo_2(\mu_3\text{-}S)_4(CuSCN)_2]$ (**5**) and $[(\eta^5\text{-}C_5Me_5)_2Mo_2(\mu_3\text{-}S)_4(CuCN)_2]\cdot CH_2Cl_2$ (**7**$\cdot CH_2Cl_2$)*

Compound **3** $\cdot 0.5CH_2Cl_2$ crystallizes in the monoclinic space group *C*2/*c* and the asymmetric unit consists of one independent $[(\eta^5\text{-}C_5Me_5)_2Mo_2(\mu_3\text{-}S)_4(CuBr)_2]$ molecule and half of the CH_2Cl_2 solvated molecule, while **5** crystallizes in the monoclinic space group *C*2/*c* and the asymmetric unit contains half of the $[(\eta^5\text{-}C_5Me_5)_2Mo_2(\mu_3\text{-}S)_4(CuSCN)_2]$ molecule, and **7** $\cdot CH_2Cl_2$ crystallizes in the orthorhombic space group *Pccn* and the asymmetric unit has half of the $[(\eta^5\text{-}C_5Me_5)_2Mo_2(\mu_3\text{-}S)_4(CuCN)_2]$ molecule and half of the CH_2Cl_2 solvated molecule. As **3**, **5** and **7** have a similar molecular structure, only the molecular structures of **5** and **7** were presented in Figs. 4 and 5. Selected bond lengths and angles of **3**, **5** and **7** are compared in Table 2.

Compounds **3**, **5** and **7** consist of a distorted $Mo_2S_4Cu_2$ cubane-like core structure in which one *cis*-$[(\eta^5\text{-}C_5Me_5)_2Mo_2(\mu\text{-}S)_2S_2]$ moiety is bound to two CuX (X = Br^-, SCN^-, CN^-) units via six Cu–S bonds . The resulting cube is closely related to those of their chloride and iodide analogues. Although there is no symmetry in **3** and its chloride and iodide analogues, there is a two-fold axis running through the center of the cube of **5** or **7**. Each Cu atom has a distorted tetrahedral coordination geometry. The mean Mo···Cu contact, Mo-μ_3-S and Cu-μ_3-S bond lengths are comparable to those found in other $Mo_2S_4Cu_2$ cubane-like clusters such as $[(dtc)_2Mo_2(\mu_3\text{-}S)_4(CuBr)_2]$ [43] and $[(\eta^5\text{-}C_5Me_5)_2Mo_2(\mu_3\text{-}S)_4(CuX)_2]$ (X=Cl, I) [40,41]. The mean Mo···Mo contact is longer than that in $[(dtc)_2Mo_2(\mu_3\text{-}S)_4(CuBr)_2]$, but comparable to those in $[(\eta^5\text{-}C_5Me_5)_2Mo_2(\mu_3\text{-}S)_4(CuX)_2]$ (X = Cl, I). Other bond lengths involved in copper(I) centers and the terminal groups are normal.

*2.4. Third-order NLO properties for **2**–**5**, **7** and $[(\eta^5\text{-}C_5Me_5)_2Mo_2(\mu_3\text{-}S)_3S(CuCl)_2]$*

As mentioned earlier in this paper, **6** has very low yield and thus we did not measure its NLO properties. On the other hand, we included the known cubane-like cluster

Table 1
Selected bond lengths (Å) and angles (°) for **2**, **4** and **6**

	2 (X = Cl)	**4** (X = Br)	**6** (X = SCN[a])
Mo(1)···Mo(2)	2.9416(7)	2.9474(7)	2.9477(12)
Mo(2)···Cu(1)	2.7202(9)	2.7230(9)	2.7100(8)
Mo(2)···Cu(2)	2.6462(7)	2.6450(7)	2.6327(8)
Mo(1)–S(1)	2.3620(13)	2.3616(12)	2.3570(12)
Mo(1)–S(2)	2.3439(10)	2.3432(9)	2.3422(13)
Mo(1)–S(4)	2.1344(11)	2.1347(10)	2.1192(13)
Mo(2)–S(1)	2.3331(10)	2.3345(9)	2.3285(12)
Mo(2)–S(2)	2.3371(12)	2.3372(11)	2.3280(12)
Mo(2)–S(3)	2.2609(11)	2.2607(10)	2.2785(12)
Cu(1)–S(1)	2.2931(11)	2.2962(11)	2.2741(13)
Cu(1)–S(3)	2.2526(11)	2.2580(10)	2.2652(14)
Cu(2)–S(2)	2.2388(11)	2.2351(10)	2.2331(13)
Cu(2)–S(3)	2.2041(13)	2.2032(12)	2.1969(14)
Cu(1)–X(1)	2.2722(12)	2.3936(7)	1.929(4)
Cu(1)–X(1A)	2.4919(14)	2.6075(11)	2.5642(14)
Cu(2)–X(2)	2.1530(11)	2.2731(7)	1.898(4)
S(1)–Mo(1)–S(2)	101.52(4)	101.37(3)	101.10(5)
S(1)–Mo(1)–S(4)	103.86(5)	103.69(4)	101.00(5)
S(2)–Mo(1)–S(4)	102.35(4)	102.23(4)	103.46(5)
S(1)–Mo(2)–S(2)	102.60(4)	102.37(3)	102.39(5)
S(1)–Mo(2)–S(3)	105.94(4)	106.03(4)	106.04(4)
S(2)–Mo(2)–S(3)	105.55(4)	105.46(4)	105.58(4)
S(1)–Cu(1)–S(3)	107.57(4)	107.41(4)	108.34(5)
S(1)–Cu(1)–X(1)	127.02(5)	127.63(3)	119.50(13)
S(1)–Cu(1)–X(1A)	109.86(5)	110.35(4)	104.63(5)
S(3)–Cu(1)–X(1)	115.77(5)	114.80(3)	119.97(13)
S(3)–Cu(1)–X(1A)	102.86(4)	102.32(3)	103.40(6)
X(1)–Cu(1)–X(1A)	89.14(4)	89.83(3)	97.64(11)
S(2)–Cu(2)–X(2)	124.56(5)	124.69(4)	119.71(14)
S(2)–Cu(2)-S(3)	110.99(5)	111.06(4)	111.82(5)
S(3)–Cu(2)–X(2)	123.93(4)	123.57(3)	128.13(14)
Cu(1)–S(3)–Cu(2)	103.35(4)	103.46(4)	102.78(6)
Cu(1)–X(1)–Cu(1A)	90.86(4)	90.17(3)	

[a] X(1) = N(1), X(1A) = S(5A), X(2) = N(2).

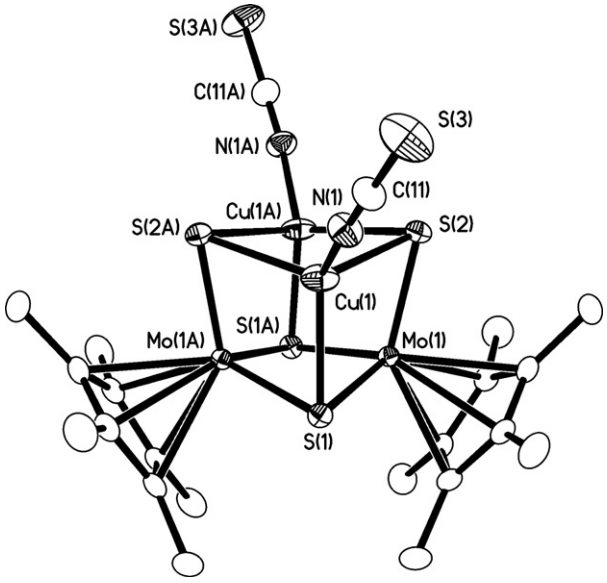

Fig. 4. Perspective view of **5** with labeling scheme and 50% thermal ellipsoids. All hydrogen atoms are omitted for charity.

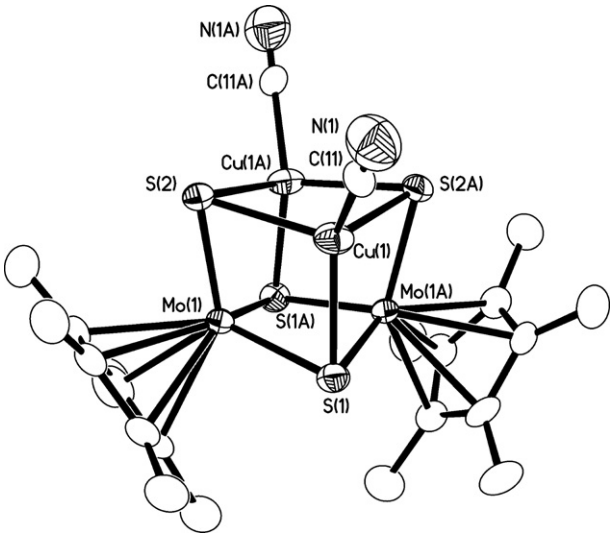

Fig. 5. Perspective view of **7** with labeling scheme and 50% thermal ellipsoids. All hydrogen atoms are omitted for charity.

$[(\eta^5\text{-}C_5Me_5)_2Mo_2(\mu_3\text{-}S)_3S(CuCl)_2]$ [40] in the measurement of third-order NLO properties of this series. As shown in Fig. 1, the UV–Vis spectra of **2**–**5** and **7** had relatively low linear absorption in 532 nm, which promises low intensity loss and little temperature change by photon absorption during their NLO measurements. The nonlinear absorption effects of **2**–**5**, **7** and $[(\eta^5\text{-}C_5Me_5)_2Mo_2(\mu_3\text{-}S)_3S(CuCl)_2]$ in CH_2Cl_2 were evaluated by the *Z*-scan technique under an open-aperture configuration (Fig. 6a, and Figs. S3a–S7a in Supplementary data). Although the detailed mechanism is still unknown, it is interesting to note that the NLO absorption data obtained under the conditions used in this study can be well described by Eqs. (1) and (2), which are derived to describe a third-order NLO process [49,50].

$$T(Z) = \frac{1}{\sqrt{\pi}q(Z)}\int_{-\infty}^{\infty}\ln[1+q(Z)]e^{-\tau^2}\,d\tau \quad (1)$$

$$q(Z) = \alpha_2 I(Z)\frac{1-e^{-\alpha_0 L}}{\alpha_0} \quad (2)$$

where light transmittance $T(Z)$ is a function of the sample's Z position (with respect to the focal point at $Z = 0$). $I(Z)$ is the incident light irradiance. α_0 and α_2 denote linear and effective third-order NLO absorptive coefficients, respectively. L is the optical path and τ is the time. The solid lines in Fig. 6a and Figs. S3a–S7a are theoretical curves from Eqs. (1) and (2). The data collected under the open aperture configuration indicated that they all exhibit good nonlinear absorption properties. The effective α_2 values for **2**–**5**, **7** and $[(\eta^5\text{-}C_5Me_5)_2Mo_2(\mu_3\text{-}S)_3S(CuCl)_2]$ are listed in Table 3.

The nonlinear refractive properties of **2**–**5**, **7** and $[(\eta^5\text{-}C_5Me_5)_2Mo_2(\mu_3\text{-}S)_3S(CuCl)_2]$ were assessed by dividing the normalized *Z*-scan data obtained under closed aperture by the normalized *Z*-scan data collected under the open aperture configuration (Fig. 6b and Figs. S3b–S7b). The

Table 2
Selected bond lengths (Å) and angles (°) for $3 \cdot 0.5CH_2Cl_2$, **5** and $7 \cdot CH_2Cl_2$[a]

$3 \cdot 0.5CH_2Cl_2$			**5**	$7 \cdot CH_2Cl_2$
Mo(1)···Mo(2)	2.8584(11)	Mo(1)···Mo(1A)	2.8508(7)	2.8655(9)
Mo(1)···Cu(1)	2.7866(14)	Mo(1)···Cu(1)	2.7970(6)	2.7847(7)
Mo(1)···Cu(2)	2.7848(14)	Mo(1)···Cu(1A)	2.7605(6)	2.7966(7)
Mo(2)···Cu(1)	2.7806(13)			
Mo(2)···Cu(2)	2.7848(16)			
Mo(1)–S(1)	2.328(2)	Mo(1)–S(1)	2.3330(7)	2.3363(11)
Mo(1)–S(2)	2.337(2)	Mo(1)–S(1A)	2.3266(8)	2.3372(12)
Mo(1)–S(3)	2.2186(19)	Mo(1)–S(2)	2.2236(7)	2.2166(12)
Mo(2)–S(1)	2.328(2)			
Mo(2)–S(2)	2.331(2)			
Mo(2)–S(4)	2.230(2)			
Cu(1)–S(1)	2.264(2)	Cu(1)–S(1)	2.2493(7)	2.2718(12)
Cu(1)–S(3)	2.403(2)	Cu(1)–S(2)	2.4538(10)	2.3926(13)
Cu(1)–S(4)	2.385(2)	Cu(1)–S(2A)	2.3774(11)	2.3848(13)
Cu(2)–S(2)	2.262(2)			
Cu(2)–S(3)	2.392(2)			
Cu(2)–S(4)	2.386(2)			
Cu(1)–X(1)	2.2650(17)	Cu(1)–X(1)	1.8833(19)	1.968(5)
Cu(2)–X(2)	2.2507(18)			
S(1)–Mo(1)–S(2)	100.64(8)	S(1)–Mo(1)–S(1A)	101.30(4)	105.12(4)
S(1)–Mo(1)–S(3)	106.39(8)	S(1)–Mo(1)–S(2)	106.66(2)	105.99(4)
S(2)–Mo(1)–S(3)	105.89(8)	S(2)–Mo(1)–S(1A)	105.93(2)	101.60(4)
S(1)–Mo(2)–S(2)	100.81(8)			
S(1)–Mo(2)–S(4)	105.97(8)			
S(2)–Mo(2)–S(4)	106.49(8)			
S(1)–Cu(1)–S(3)	102.53(8)	S(1)–Cu(1)–S(2)	101.92(2)	102.42(4)
S(1)–Cu(1)–S(4)	103.04(8)	S(1)–Cu(1)–S(2A)	103.44(2)	101.88(4)
S(1)–Cu(1)–X(1)	124.43(8)	S(1)–Cu(1)–X(1)	121.53(7)	127.63(13)
S(3)–Cu(1)–S(4)	98.35(8)	S(2)–Cu(1)–S(2A)	100.07(4)	102.18(4)
S(3)–Cu(1)–X(1)	110.14(8)	S(2)–Cu(1)–X(1)	109.87(7)	108.15(13)
S(4)–Cu(1)–X(1)	114.72(8)	S(2A)–Cu(1)–X(1)	117.01(7)	111.60(12)
S(2)–Cu(2)–S(3)	102.71(8)			
S(2)–Cu(2)–S(4)	103.66(9)			
S(2)–Cu(2)–X(2)	123.72(8)			
S(3)–Cu(2)–S(4)	98.64(8)			
S(3)–Cu(2)–X(2)	110.38(8)			
S(4)–Cu(2)–X(2)	114.35(8)			

[a] X = Br (**3**); X(1) = N(1) (**5**); X(1) = C(11) ($7 \cdot CH_2Cl_2$).

effective third-order NLO refractive indexes n_2 can be derived from the difference between normalized transmittance values at valley and peak positions (ΔT_{V-P}) by using Eq. (3) [51,52]:

$$n_2 = \frac{\lambda\alpha_0}{0.812\pi I(1-e^{-\alpha_0 L})}\Delta T_{V-P} \quad (3)$$

where λ is the wavelength of the laser, α_0 is the linear coefficient, L is the sample thickness, I is the peak irradiation intensity at focus. As shown in Table 3, the effective third-order NLO refractive indexes n_2 values are negative, indicating that they all show strong self-defocusing effect.

In accordance with the observed α_2 and n_2 values, the effective third-order susceptibility $\chi^{(3)}$ and the hyperpolarizability γ value can be calculated by Eqs. (4) and (5) [51,52]:

$$|\chi^{(3)}| = \sqrt{\left(\left|\frac{9\times10^8\varepsilon_0 n_0^2 c^2}{2v}\alpha_2\right|^2 + \left|\frac{cn_0^2 n_2}{80\pi}\right|^2\right)} \quad (4)$$

$$\gamma = \chi^{(3)}/NF^4 \quad (5)$$

where c is speed of light in vacuum, n_0 is linear refractive indexes of the sample. N is the number density (concentration) of the clusters in the samples; F^4 (=3.25) is the local field correction factor. Table 3 lists the effective third-order susceptibilities $\chi^{(3)}$ that are calculated by Eq. (4). These results showed that **2**–**5**, **7** and $[(\eta^5\text{-}C_5Me_5)_2Mo_2(\mu_3\text{-}S)_3S(CuCl)_2]$ possess strong third-order optical nonlinearities.

According to Eq. (5), N represents the number density (concentration) of a compound. Therefore the hyperpolarizability γ value can be used to represent NLO properties of neat materials. Table 4 lists the γ values of **2**–**5**, **7**, $[(\eta^5\text{-}C_5Me_5)_2Mo_2(\mu_3\text{-}S)_3S(CuCl)_2]$ and some reported NLO materials for comparison. The γ values of **2**–**5**, **7** and $[(\eta^5\text{-}C_5Me_5)_2Mo_2(\mu_3\text{-}S)_3S(CuCl)_2]$ are comparable to those of the Mo/S/Cu clusters [32,51,53–55], better than those observed in C_{60} and C_{70} [56], organometallic compounds and their films like TiOPc [57,58]. It is noticed that the γ values of the single cubane-like clusters ($[(\eta^5\text{-}C_5Me_5)_2Mo_2(\mu_3\text{-}S)_3S(CuCl)_2]$, **3**, **5**, and **7**) are 2–4 times larger, while those of the double incomplete cubane-like

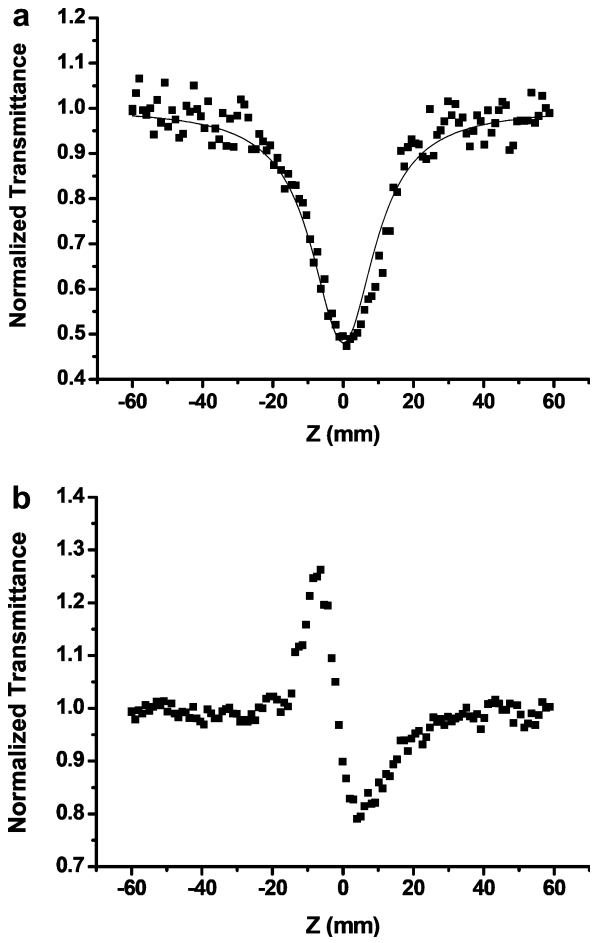

Fig. 6. *Z*-scan data of 5.13×10^{-4} M CH_2Cl_2 of **4** at 532 nm. (a) The data were evaluated under the open aperture configuration. (b) The data were assessed by dividing the normalized *Z*-scan data obtained under the closed aperture by the normalized *Z*-scan data in (a). The black dots are the experimental data, and the solid curve is the theoretical fit.

clusters (**2** and **4**) are nearly 8 times larger than that of their precursor [(η^5-C_5Me_5)$_2$$Mo_2$($\mu$- S)$_2$$S_2$]. These enhancements in γ value may be ascribed to skeletal extension of metal cluster [30,59,60]. Among these single cubane-like clusters, the γ values seem not get much changed though each cluster has its own distinct periphery X groups around its [(η^5-C_5Me_5)$_2$$Mo_2$($\mu_3$-S)$_3$$SCu_2$] core. The same thing occurred for the double incomplete cubane-like clusters **2** and **4**. However, the γ values of the double incomplete cubane-like clusters (**2** and **4**) are about 2 times larger than those of the corresponding single cubane-like clusters ([(η^5-C_5Me_5)$_2$-Mo_2(μ_3-S)$_3$S$(CuCl)_2$] and **3**). This improvement may be due to the existence of the double incomplete cubane-like cluster framework of **2** and **4**.

3. Experimental

3.1. General

All manipulations were performed under an argon atmosphere using standard Schlenk-line techniques. Compound **1** was prepared according to the literature method [40]. CH_3CN was pre-dried over activated molecular sieves and refluxed over P_2O_5 under argon. All other chemicals were used as purchased. ^{1}H NMR spectra were recorded at ambient temperature on a Varian UNITY plus-400 spectrometer where the chemical shifts were referenced to TMS in $CDCl_3$. IR spectra were recorded on a Varian Scimitar 1000 spectrometer (4000–400 cm^{-1}). Elemental analyses for C, H and N were performed on a Carlo-Erba CHNO-S microanalyzer. Electronic spectra were measured on a Varian Cary 50 UV–Vis spectrophotometer.

3.2. Syntheses

3.2.1. Reactions of *1* with CuCl

A suspension containing **1** (30 mg, 0.05 mmol) and CuCl (10 mg, 0.10 mmol) in 4 mL of CH_3CN was refluxed for 20 h, forming a dark green solution. After cooling to room temperature, the resulting mixture was concentrated to dryness in vacuo, and the components were separated by column chromatography on silica. Elution with CH_2Cl_2/Et_2O (8:1) gave a dark brown band first. The solution was concentrated to ca. 2 mL in vacuo and then layered by Et_2O (8 mL) for two weeks to form dark brown needles of **2**. Yield: 20 mg (51% based on Mo). The component in the second green band was eluted with acetone/CH_2Cl_2 (1:4). A similar workup to that used in the isolation of **2** produced dark green prisms of [(η^5-C_5Me_5)$_2$$Mo_2$($\mu_3$-S)$_4$$(CuCl)_2$]. Yield: 13 mg (33% based on Mo). Anal. Calc. for $C_{40}H_{60}Cl_4Cu_4Mo_4S_8$ (**2**): C, 30.46; H, 3.83. Found: C, 30.02; H, 4.06%. IR (KBr disk): 2955 (m), 2900 (m), 1626 (m), 1475 (m), 1422 (m), 1378 (s), 1022 (m), 503 (s), 428 (m) cm^{-1}. UV–Vis (CH_2Cl_2, λ_{max} (nm (ε M^{-1} cm^{-1}))): 259 (54,200), 320 (27,800), 350 (24,600), 491 (7300). ^{1}H NMR ($CDCl_3$, 400 MHz, ppm): δ 2.06 (s, 30H, –CH_3), 2.29 (s, 30H, –CH_3).

Table 3
NLO parameters of **2**–**5**, **7** and [(η^5-C_5Me_5)$_2$$Mo_2$($\mu_3$- S)$_4$$(CuCl)_2$]

Compounds	c ($\times 10^{-4}$ M)	α_2 ($\times 10^{-10}$ m/W)	n_2 ($\times 10^{-11}$ esu)	$\chi^{(3)}$ ($\times 10^{-11}$ esu)
[(η^5-C_5Me_5)$_2$$Mo_2$($\mu_3$- S)$_4$$(CuCl)_2$]	10.7	7.58	−12.08	2.49
2	5.11	8.77	−16.95	2.90
3	9.82	6.10	−11.72	2.01
4	5.13	7.49	−17.59	2.49
5	4.80	3.80	−7.54	1.25
7	12.5	5.50	−11.59	1.82

Table 4
Comparison of the γ values of **2**–**5**, **7** and some known NLO materials

Compounds	γ (esu)	λ (nm)	Ref.
$[(\eta^5\text{-}C_5Me_5)_2Mo_2(\mu_3\text{-}S)_4(CuCl)_2]$	1.19×10^{-29}	532	This work
2	2.84×10^{-29}	532	This work
3	1.05×10^{-29}	532	This work
4	2.48×10^{-29}	532	This work
5	1.34×10^{-29}	532	This work
7	7.45×10^{-30}	532	This work
$[(\eta^5\text{-}C_5Me_5)_2Mo_2(\mu\text{-}S)_2S_2]$	3.07×10^{-30}	532	[41]
$[(\eta^5\text{-}C_5Me_5)_2Mo_2(\mu_3\text{-}S)_3S(CuI)_2]$	5.65×10^{-30}	532	[41]
$[(\eta^5\text{-}C_5Me_5)_2Mo_2(\mu_3\text{-}S)_4(CuI)_2]$	1.18×10^{-29}	532	[41]
$[(n\text{-}Bu)_4N]_2[MoOS_3(CuNCS)_3]$	4.8×10^{-29}	532	[32]
$[MoS_4Cu_4(\alpha\text{-}MePy)_5Br_2]\cdot 2(\alpha\text{-}MePy)_{0.5}$	1.06×10^{-31}	532	[53]
$\{[MoS_4Cu_4(\alpha\text{-}MePy)_3Br](\mu\text{-}Br)\cdot(\alpha\text{-}MePy)\}_n$	1.02×10^{-31}	532	[53]
$[MoOS_3Cu_3(4\text{-}pic)_6]\cdot[BF_4]$	2.89×10^{-31}	532	[54]
$[MoOS_3Cu_3(4\text{-}pic)_6]\cdot 0.5[Mo_2O_7]$	1.32×10^{-30}	532	[54]
$(Et_4N)_3[WOS_3(CuBr)_3(\mu_2\text{-}Br)]\cdot 2H_2O$	0.6×10^{-28}	532	[51]
$[Et_4N]_2[MoS_4Cu_4(SCN)_4(2\text{-}pic)_4]$[a]	0.29×10^{-31}	532	[55]
C_{60}	7.5×10^{-34}	1910	[56]
C_{70}	1.3×10^{-33}	1910	[56]
$VOPcBu_4$ (PMMA doped film)[b]	8×10^{-34}	1907	[57]
TiOPc (film before thermal annealing)	1.04×10^{-33}	1907	[58]
TiOPc (film after thermal annealing)	5.35×10^{-34}	1907	[58]

[a] pic = methylpyradine (picoline).
[b] Pc = phthalocyanine.

*3.2.2. Reactions of **1** with CuBr*

The similar reactions of **1** (30 mg, 0.05 mmol) with CuBr (15 mg, 0.10 mmol) followed by column chromatography on silica using CH_2Cl_2/Et_2O (8:1) led to the formation of dark-green needles of $\mathbf{3}\cdot 0.5CH_2Cl_2$ and dark-brown prisms of **4**, respectively. Yield: 21 mg (46% based on Mo) for $\mathbf{3}\cdot 0.5CH_2Cl_2$ and 13 mg (30% based on Mo) for **4**. Anal. Calc. for $C_{20.5}H_{31}Br_2ClCu_2Mo_2S_4$ ($\mathbf{3}\cdot 0.5CH_2Cl_2$): C, 26.76; H, 3.40. Found: C, 26.13; H, 3.77%. IR (KBr disk): 2956 (m), 2911 (m), 1624 (m), 1477 (m), 1421 (m), 1380 (s), 1020 (m), 451 (m) cm^{-1}. UV–Vis (CH_2Cl_2, λ_{max} (nm (ε $M^{-1}\,cm^{-1}$))): 296 (21,000), 393 (4400), 474 (2000). ^1H NMR ($CDCl_3$, 400 MHz, ppm): δ 2.09 (s, 30H, $-CH_3$). Anal. Calc. for $C_{40}H_{60}Br_4Cu_4Mo_4S_8$ (**4**): C, 27.37; H, 3.45. Found: C, 27.58; H, 3.72%. IR (KBr disk): 2955 (m), 2906 (m), 1621 (m), 1475 (m), 1422 (m), 1378 (s), 1020 (m), 503 (s), 428 (s) cm^{-1}. UV–Vis (CH_2Cl_2, λ_{max} (nm (ε $M^{-1}\,cm^{-1}$))): 260 (56,300), 326 (30,900), 352 (27,600), 491 (7700). ^1H NMR ($CDCl_3$, 400 MHz, ppm): δ 2.06 (s, 30H, $-CH_3$), 2.28 (s, 30H, $-CH_3$).

*3.2.3. Reactions of **1** with CuSCN*

A suspension containing **1** (60 mg, 0.1 mmol) and CuSCN (25 mg, 0.2 mmol) in 8 mL of CH_3CN was refluxed for 20 h, forming a brown solution with a lot of dark brown solid. After cooling to room temperature, the solution was concentrated to dryness in vacuo and then extracted by CH_2Cl_2 (2 mL × 3). The components in the resulting brown extract was separated by column chromatography on silica using Et_2O/CH_2Cl_2 (1:8). Similar workups to those used in the isolation of $[(\eta^5\text{-}C_5Me_5)_2Mo_2(\mu_3\text{-}S)_4(CuCl)_2]$ and **2** gave rise to dark green prisms of **5** and dark brown prisms of **6**, respectively. Yield: 26 mg (31% based on Mo) for **5** and 1.5 mg (2% based on Mo) for **6**. Anal. Calc. for $C_{22}H_{30}Cu_2Mo_2N_2S_6$ (**5**): C, 31.69; H, 3.63; N, 3.36. Found: C, 31.95; H, 3.81; N, 3.51%. IR (KBr disk): 2959 (w), 2911 (m), 2093 (s), 1630 (m), 1478 (m), 1423 (m), 1378 (s), 1020 (m), 454 (m) cm^{-1}. UV–Vis (CH_2Cl_2, λ_{max} (nm (ε $M^{-1}\,cm^{-1}$))): 291 (21,100), 387 (5100), 468 (2700). ^1H NMR ($CDCl_3$, 400 MHz, ppm): δ 2.12 (s, 30H, $-CH_3$). Anal. Calc. for $C_{44}H_{60}Cu_4Mo_4N_4S_{12}$ (**6**): C, 31.69; H, 3.63, N, 3.36. Found: C, 32.03; H, 3.88, N, 3.55%. IR (KBr disk): 2956 (w), 2907 (m), 2115 (m), 2078 (s), 1625 (m), 1477 (m), 1426 (m), 1377 (s), 1022 (m), 498 (m), 455 (w) cm^{-1}. UV–Vis (CH_2Cl_2, λ_{max} (nm (ε $M^{-1}\,cm^{-1}$))): 267 (47,300), 326 (26,600), 469 (12,300). ^1H NMR ($CDCl_3$, 400 MHz, ppm): δ 2.06 (s, 30H, $-CH_3$), 2.17 (s, 30H, $-CH_3$).

*3.2.4. Reactions of **1** with CuCN*

A suspension containing **1** (30 mg, 0.05 mmol) and CuCN (9 mg, 0.1 mmol) in 6 mL of CH_3CN was refluxed for 20 h, forming a greenish brown solution with a large amount of dark brown solid. Similar workups to those mentioned above produced dark-green prisms of $\mathbf{7}\cdot CH_2Cl_2$ and some unreacted **1**. Yield: 10 mg (23% based on Mo) for $\mathbf{7}\cdot CH_2Cl_2$. Anal. Calc. for $C_{23}H_{32}Cl_2Cu_2Mo_2N_2S_4$: C, 32.32; H, 3.77; N, 3.28. Found: C, 33.03; H, 3.92; N, 3.35%. IR (KBr disk): 2958 (m), 2913 (m), 2154 (m), 2087 (s), 1628 (m), 1480 (m), 1423 (m), 1376 (s), 1021 (m), 455 (m) cm^{-1}. UV–Vis (CH_2Cl_2, λ_{max}(nm (ε $M^{-1}\,cm^{-1}$))): 291 (20,800), 456 (2200). ^1H NMR ($CDCl_3$, 400 MHz, ppm): δ 2.08 (s, 30H, $-CH_3$).

Table 5
Crystallographic data for **2**–**7**

	2	**3** · $0.5CH_2Cl_2$	**4**	**5**	**6**	**7** · CH_2Cl_2
Chemical formula	$C_{40}H_{60}Cl_4Cu_4Mo_4S_8$	$C_{20.5}H_{31}Br_2ClCu_2Mo_2S_4$	$C_{40}H_{60}Br_4Cu_4Mo_4S_8$	$C_{22}H_{30}Cu_2Mo_2N_2S_6$	$C_{44}H_{60}Cu_4Mo_4N_4S_{12}$	$C_{23}H_{32}Cl_2Cu_2Mo_2N_2S_4$
Formula weight	1577.08	919.93	1754.92	833.80	1667.60	854.61
Crystal system	Monoclinic	Monoclinic	Monoclinic	Monoclinic	Monoclinic	Orthorhombic
Space group	$P2_1/c$	$C2/c$	$P2_1/c$	$C2/c$	$P2_1/c$	$Pccn$
a (Å)	16.574(3)	36.684(7)	16.787(3)	23.890(5)	12.175(2)	13.002(3)
b (Å)	10.135(2)	10.354(2)	10.212(2)	8.7466(17)	14.193(3)	13.028(3)
c (Å)	17.390(4)	16.114(3)	17.468(4)	17.717(4)	17.309(4)	18.113(4)
β (°)	117.10(3)	108.68(3)	116.73(3)	128.34(3)	104.68(3)	
V (Å^3)	2600.4(9)	5798(2)	2674.4(9)	2903.8(10)	2893.4(10)	3068.1(11)
Z	2	8	2	4	2	4
D_{calc} (g cm^{-3})	2.014	2.108	2.179	1.907	1.914	1.850
$F(000)$	1560	3576	1704	1656	1656	1696
μ (Mo Kα, cm^{-1})	3.091	5.439	5.794	2.736	2.746	2.629
Total number of reflections	25111	31577	28943	15445	28272	28380
Number of unique reflections	4755	6624	6108	3330	5275	2798
Number of observed reflections [$I > 2.00\sigma(I)$]	4338	5947	5722	3189	4667	2616
Number of variables	281	299	281	159	317	164
R[a]	0.0310	0.0754	0.0320	0.0237	0.0385	0.0421
wR[b]	0.0630	0.2153	0.0752	0.0567	0.0760	0.0962
GOF[c]	1.163	1.062	1.130	1.094	1.167	1.246
Residual peaks (e/Å^3)	0.640, −0.528	1.145, −1.750	0.643, −1.294	0.490, −0.778	0.728, −0.600	0.795, −0.698

[a] $R = \sum||F_o| - |F_c|/\sum|F_o|$.
[b] $wR = \{\sum w(F_o^2 - F_c^2)^2/\sum w(F_o^2)^2\}^{1/2}$.
[c] GOF $= \{\sum[w((F_o^2 - F_c^2)^2)/(n-p)\}^{1/2}$, where n = number of reflections and p = total numbers of parameters refined.

3.3. X-ray crystallography

All measurements were performed on a Rigaku Mercury CCD X-ray diffractometer (3KV, sealed tube) at −80°C, using graphite monochromated Mo Kα ($\lambda = 0.71070$ Å). A dark-brown needle of **2** with dimensions $0.21 \times 0.15 \times 0.12$ mm, a dark-green needle of $\mathbf{3} \cdot 0.5CH_2Cl_2$ with dimensions $0.28 \times 0.27 \times 0.15$ mm, a dark-brown prism of **4** with dimensions $0.68 \times 0.41 \times 0.30$ mm, a dark-green prism of **5** with dimensions $0.42 \times 0.17 \times 0.15$ mm, a dark-brown prism of **6** with dimensions $0.20 \times 0.12 \times 0.11$ mm and a dark-green prism of $\mathbf{7} \cdot CH_2Cl_2$ with dimensions $0.25 \times 0.24 \times 0.10$ mm were mounted on glass fibers with grease, respectively. Diffraction data were collected at ω mode with a detector distance of 35 mm to the crystal. Indexing was performed from six images, each of which was exposed for 15 s. A total of 720 oscillation images for each were collected in the range $6.10° < 2\theta < 50.70°$ for **2**, $6.40° < 2\theta < 54.96°$ for $\mathbf{3} \cdot 0.5CH_2Cl_2$, $6.14° < 2\theta < 54.96°$ for **4**, $6.56° < 2\theta < 54.94°$ for **5**, $6.24° < 2\theta < 50.70°$ for **6** and $6.26° < 2\theta < 50.70°$ for $\mathbf{7} \cdot CH_2Cl_2$. The collected data were reduced by using the program CrystalClear (Rigaku and MSC, Ver. 1.3, 2001), and an absorption correction (multi-scan) was applied, which resulted in transmission factors raging from 0.563 to 0.708 for **2**, from 0.311 to 0.496 for $\mathbf{3} \cdot 0.5CH_2Cl_2$, 0.110–0.275 for **4**, 0.393–0.684 for **5**, 0.610–0.752 for **6** and 0.559–0.779 for $\mathbf{7} \cdot CH_2Cl_2$. The reflection data were also corrected for Lorentz and polarization effects.

The crystal structures of **2**, $\mathbf{3} \cdot 0.5CH_2Cl_2$, **4**–**6** and $\mathbf{7} \cdot CH_2Cl_2$ were solved by direct methods [61], and expanded using Fourier techniques [62]. All non-hydrogen atoms were refined anisotropically. The CH_2Cl_2 molecule in $\mathbf{3} \cdot 0.5CH_2Cl_2$ were found to be disordered over three sites with occupancy factors of 0.74/0.13/0.13 for C21/C21A/C21B, Cl1/Cl1B/Cl1A and Cl1C/Cl1A/Cl1D. All hydrogen atoms except those of the disordered CH_2Cl_2 molecule were placed in geometrically idealized positions (C–H = 0.98 Å for methyl groups and C–H = 0.99 Å for methylene groups) and constrained to ride on their parent atoms with $U_{iso}(H) = 1.2U_{eq}(C)$. All the calculations were performed on a Dell workstation using the CrystalStructure crystallographic software package (Rigaku/MSC, Ver. 3.60, 2004). Important crystal and data collection parameters for **2**, $\mathbf{3} \cdot 0.5CH_2Cl_2$, **4**–**6** and $\mathbf{7} \cdot CH_2Cl_2$ are summarized in Table 5.

3.4. Nonlinear optical measurements

The solutions of **2**–**7** along with $[(\eta^5\text{-}C_5Me_5)_2Mo_2(\mu_3\text{-}S)_4(CuCl)_2]$ in CH_2Cl_2 were placed in 2-mm quartz cuvette for NLO measurements. The clusters were stable toward air and laser light in experimental condition. The nonlinear absorption and refraction were investigated with a linearly polarized laser light ($\lambda = 532$ nm; pulse widths = 8 ns; repetition rate = 1 Hz) provided by a frequency-doubled, mode-locked, Q-switched Nd-YAG laser. The spatial profiles of the optical pulses were nearly gaussian after passing through a spatial filter. The laser beam was focused with a 30-cm focal length focusing mirror. The radius of the beam waist was measured to be 35 ± 5 μm (half-width at $1/e^2$ maximum). The incident and transmitted pulse energies were measured simultaneously by two energy detectors (Laser Precision Rjp-735), which were linked to a computer by an IEEE interface [49,50]. The NLO properties of the samples were manifested by moving the samples along the axis of the incident laser irradiance beam (z-direction) with respect to the focal point and with incident laser irradiance kept constant (Z-scan methods). The closed-aperture curves are normalized to the open aperture curves. An aperture of 0.2 mm radius was placed in front of the detector to measure the transmitted energy when assessment of laser beam distortion was needed. To eliminate scattering effects, a lens was mounted after the samples to collected the scattered light.

Acknowledgements

This work was supported by the NNSF of China (No. 20525101), the NSF of Jiangsu Province (No. BK2004205), the Specialized Research Fund for the Doctoral Program of Higher Education (No. 20050285004), the Qin-Lan Project of Jiangsu Province, and the State Key Laboratory of Organometallic Chemistry of SIOC (No. 06-26) in China.

Appendix A. Supplementary data

CCDC 616452, 616453, 616454, 616455, 616456 and 616457 contain the supplementary crystallographic data for **2**, $\mathbf{3} \cdot 0.5CH_2Cl_2$, **4**, **5**, **6** and $\mathbf{7} \cdot CH_2Cl_2$. These data can be obtained free of charge via http://www.ccdc.cam.ac.uk/conts/retrieving.html, or from the Cambridge Crystallographic Data Centre, 12 Union Road, Cambridge CB2 1EZ, UK; fax: (+44) 1223-336-033; or e-mail: deposit@ccdc.cam.ac.uk. Supplementary data associated with this article can be found, in the online version, at doi:10.1016/j.jorganchem.2007.01.040.

References

[1] A. Müller, E. Diemann, R. Jostes, H. Bögge, Angew. Chem. Int. Ed. 20 (1981) 934.
[2] A. Müller, H. Bögge, U. Schimanski, M. Penk, K. Nieradzik, M. Dartmann, E. Krickemeyer, J. Schimanski, C. Römer, M. Römer, H. Dornfeld, U. Wienböker, W. Hellmann, Monatsh. Chem. 120 (1989) 367.
[3] S. Sarkar, S.B.S. Mishra, Coord. Chem. Rev. 59 (1984) 239.
[4] Y. Jeannin, F. Sécheresse, S. Bernés, F. Robert, Inorg. Chim. Acta 198–200 (1992) 493.
[5] E.I. Stiefel, D. Coucouvanis, W.E. Newton, in: Molybdenum Enzymes Cofactors and Model SystemsACS Symp. Ser., 535, Am. Chem. Soc., Washington, DC, 1993.
[6] E.I. Stiefel, K. Matsumoto, in: Transition Metal Sulfur Chemistry, Biological and Industrial SignificanceACS Symp. Ser., 653, Am. Chem. Soc., Washington, DC, 1996.

[7] X.T. Wu, P.C. Chen, S.W. Du, N.Y. Zhu, J.X. Lu, J. Cluster Sci. 5 (1994) 265.
[8] D.X. Wu, M.C. Hong, R. Cao, H.Q. Liu, Inorg. Chem. 35 (1996) 1080.
[9] W.J. Zhang, A. Behrens, J. Gätjens, M. Ebel, X.T. Wu, D. Rehder, Inorg. Chem. 43 (2004) 3020.
[10] S. Ogo, T. Suzuki, Y. Ozawa, K. Isobe, Inorg. Chem. 35 (1996) 6093.
[11] C.M. Che, B.H. Xia, J.S. Huang, C.K. Chan, Z.Y. Zhou, K.K. Cheung, Chem. Eur. J. 7 (2001) 3998.
[12] J.G. Li, X.Q. Xin, Z.Y. Zhou, K.B. Yu, J. Chem. Soc. Chem. Commun. (1990) 250.
[13] J.P. Lang, X.Q. Xin, J. Solid State Chem. 108 (1994) 118.
[14] J.P. Lang, K. Tatsumi, Inorg. Chem. 37 (1998) 6308.
[15] H.W. Hou, H.G. Zheng, G.A. How, Y.F. Fan, M.K.M. Low, Z. Yu, W.L. Wang, X.Q. Xin, W. Ji, W.T. Wong, J. Chem. Soc., Dalton Trans. (1999) 2953.
[16] H. Yu, Q.F. Xu, Z.R. Sun, S.J. Ji, J.X. Chen, Q. Liu, J.P. Lang, K. Tatsumi, Chem. Commun. (2001) 2614.
[17] J.P. Lang, Q.F. Xu, R.X. Yuan, B.F. Abrahams, Angew. Chem. Int. Ed. 43 (2004) 4741.
[18] J.P. Lang, C.M. Jiao, S.B. Qiao, W.H. Zhang, B.F. Abrahams, Inorg. Chem. 44 (2005) 3664.
[19] J.P. Lang, H. Kawaguchi, S. Ohnishi, K. Tatsumi, Chem. Commun. (1997) 405.
[20] J.P. Lang, K. Tatsumi, Inorg. Chem. 37 (1998) 160.
[21] J.P. Lang, H. Kawaguchi, S. Ohnishi, K. Tatsumi, Inorg. Chim. Acta 283 (1998) 136.
[22] J.P. Lang, K. Tatsumi, J. Organomet. Chem. 579 (1999) 332–337.
[23] J.P. Lang, H. Kawaguchi, K. Tatsumi, Chem. Commun. (1999) 2315.
[24] J.P. Lang, Q.F. Xu, Z.N. Chen, B.F. Abrahams, J. Am. Chem. Soc. 125 (2003) 12682.
[25] J.P. Lang, S.J. Ji, Q.F. Xu, Q. Shen, K. Tatsumi, Coord. Chem. Rev. 241 (2003) 47.
[26] J.P. Lang, Q.F. Xu, W. Ji, H.I. Elim, K. Tatsumi, Eur. J. Inorg. Chem. (2004) 86.
[27] Q.F. Xu, J.X. Chen, W.H. Zhang, Z.G. Ren, H.X. Li, Y. Zhang, J.P. Lang, Inorg. Chem. 45 (2006) 4055.
[28] G.N. George, I.J. Pickering, E.Y. Yu, R.C. Prince, S.A. Bursakov, O.Y. Gavel, I. Moura, J.J.G. Moura, J. Am. Chem. Soc. 122 (2000) 8321.
[29] E.K. Quagraine, R.S. Reid, J. Inorg. Biochem. 85 (2001) 53.
[30] S. Shi, W. Ji, S.H. Tang, J.P. Lang, X.Q. Xin, J. Am. Chem. Soc. 116 (1994) 3615.
[31] S. Shi, W. Ji, J.P. Lang, X.Q. Xin, J. Phys. Chem. 98 (1994) 3570.
[32] S. Shi, W. Ji, W. Xie, S.H. Tang, H.C. Zeng, J.P. Lang, X.Q. Xin, Mater. Chem. Phys. 39 (1995) 298.
[33] H.G. Zheng, W. Ji, M.L.K. Low, G. Sakane, T. Shibahara, X.Q. Xin, J. Chem. Soc., Dalton Trans. (1997) 2375.
[34] S. Shi, in: D.M. Roundhill, J.P. FacklerJr. (Eds.), Optoelectronic Properties of Inorganic Compounds, Plenum Press, New York, 1998, pp. 55–105.
[35] C. Zhang, Y.L. Song, B.M. Fung, Z.L. Xue, X.Q. Xin, Chem. Commun. (2001) 843.
[36] X.R. Zhu, R.M. Niu, Z.R. Sun, H.P. Zeng, Z.G. Wang, J.P. Lang, Chem. Phys. Lett. 372 (2003) 524.
[37] X.R. Zhu, Z.R. Sun, R.M. Niu, H.P. Zeng, Z.G. Wang, J.P. Lang, Z.Z. Xu, R.X. Li, J. Appl. Phys. 94 (2003) 4772.
[38] B.J. Coe, in: J.A. McCleverty, T.J. Meyer (Eds.), Comprehensive Coordination Chemistry II, vol. 9, Elsevier Pergamon, Oxford, UK, 2004, pp. 621–687.
[39] H. Yu, W.H. Zhang, Z.G. Ren, J.X. Chen, C.L. Wang, J.P. Lang, H.I. Elim, W. Ji, J. Organomet. Chem. 690 (2005) 4027.
[40] H. Brunner, R. Graßbl, J.J. Wachter, Organomet. Chem. 393 (1990) 119.
[41] Z.G. Ren, H.X. Li, G.F. Liu, W.H. Zhang, J.P. Lang, Y. Zhang, Y.L. Song, Organometallics 25 (2006) 4351.
[42] J.P. Lang, H. Kawaguchi, K. Tatsumi, Dalton Trans. (2002) 2573.
[43] Z.H. Wei, Q.F. Xu, H.X. Li, J.X. Chen, J.P. Lang, J. Organomet. Chem. 687 (2003) 197.
[44] J.M. Manoli, C. Potvin, F. Sécheresse, S. Marzak, Inorg. Chim. Acta 150 (1988) 257.
[45] A.E. Bruce, D.R. Tyler, Inorg. Chem. 23 (1984) 3433.
[46] H. Kawaguchi, K. Yamada, J.-P. Lang, K. Tatsumi, J. Am. Chem. Soc. 119 (1997) 10346.
[47] J.G. Li, F.J. Gao, J.P. Lang, X.Q. Xin, K.B. Yu, Chin. J. Struct. Chem. 11 (1992) 351.
[48] W. Clegg, C.D. Garner, J.R. Nichlson, P.R. Raithby, Acta Crystallogr., Sect. C: Cryst. Struct. Commun. 39 (1983) 1007.
[49] M. Sherk-Bahae, A.A. Said, T.H. Wei, D.J. Hagan, E.W. Van Stryland, IEEE J. Quantum Electron. 26 (1990) 760.
[50] M. Sherk-Bahae, A.A. Said, E.W. Van Stryland, Opt. Lett. 14 (1989) 955.
[51] Z.R. Chen, H.W. Hou, X.Q. Xin, K.B. Yu, S. Shi, J. Phys. Chem. 99 (1995) 8717.
[52] L. Yang, R. Dorsinville, Q.Z. Wang, P.X. Ye, R.R. Alfano, R. Zamboni, C. Taliani, Opt. Lett. 17 (1992) 323.
[53] W.H. Zhang, J.X. Chen, H.X. Li, B. Wu, X.Y. Tang, Z.G. Ren, Y. Zhang, J.P. Lang, Z.R. Sun, J. Organomet. Chem. 690 (2005) 394.
[54] C. Zhang, Y.L. Song, F.E. Kühn, Y. Xu, X.Q. Xin, H.K. Fun, W.A. Herrmann, Eur. J. Inorg. Chem. (2002) 55.
[55] C. Zhang, Y.L. Song, G.C. Jin, G.Y. Feng, Y.X. Wang, S.S.S. Rag, H.K. Fun, X.Q. Xin, J. Chem. Soc., Dalton. Trans. (2000) 1317.
[56] Y. Wang, L.T. Cheng, J. Phys. Chem. 96 (1992) 1530.
[57] M. Hosoda, T. Wada, A. Yamada, A.F. Garito, H. Sasabe, Mater. Res. Soc. Symp. Proc. 175 (1990) 89.
[58] M. Hosoda, T. Wada, A. Yamada, A.F. Garito, Jpn. J. Appl. Phys. 30 (1991) L1486.
[59] S. Shi, Z. Lin, Y. Mo, X.Q. Xin, J. Phys. Chem. 100 (1996) 10695.
[60] Q.F. Zhang, Y.Y. Niu, W.H. Lueng, Y.L. Song, I.D. Williams, X.Q. Xin, Chem. Commun. (2001) 1126.
[61] G.M. Sheldrick, SHELXS-97, Program for the Solution of Crystal Structure, University of Goettingen, Germany, 1997.
[62] P.T. Beurskens, G. Admiraal, G. Beurskens, W.P. Bosman, R. de Gelder, R. Israel, J.M.M. Smits, DIRDIF99, The DIRDIF-99 Program System, Technical Report of the Crystallography Laboratory, University of Nijmegen, The Netherlands, 1999.